Combined DiI and antibody labeling reveals complex dysgenesis of hippocampal spine synapses in a mouse model of Fragile X Syndrome

Luisa Speranza [1]*, Kardelen Dalım Filiz [2], Sarah Goebel [1], Carla Perrone-Capano [2], Salvatore Pulcrano [3], Floriana Volpicelli [2]†, and Anna Francesconi [1]*†

[1] Dominick P. Purpura Department of Neuroscience, Albert Einstein College of Medicine, New York, NY 10461 US; luisa.speranza@einsteinmed.edu; Sarah.Goebel@einsteinmed.edu; anna.francesconi@einsteinmed.edu

[2] Department of Pharmacy, School of Medicine and Surgery, University of Naples Federico II, 80131, Naples, Italy; kardelendalim@gmail.com; perrone@unina.it; floriana.volpicelli@unina.it

[3] Institute of Genetics and Biophysics "A. Buzzati-Traverso", C.N.R., 80131 Naples, Italy; salvatore.pulcrano@igb.cnr.it

*Correspondence: Anna Francesconi, Ph.D. anna.francesconi@einsteinmed.edu; Luisa Speranza, Ph.D. luisa.speranza@einsteinmed.edu

† These authors contributed equally.

Abstract: Structural, functional, and molecular alterations in excitatory spine synapses are a common hallmark of many neurodevelopmental disorders including intellectual disability and autism. Here, we describe an optimized methodology, based on combined use of DiI and immunofluorescence, for rapid and sensitive characterization of the structure and composition of spine synapses in native brain tissue. We successfully demonstrate the applicability of this approach by examining the properties of hippocampal spine synapses in juvenile *Fmr1* KO mice, a mouse model of Fragile X Syndrome. We find that mutant mice display pervasive dysgenesis of spine synapses evidenced by an overabundance of both abnormally elongated thin spines and cup-shaped spines, in combination with reduced density of mushroom spines. We further find that mushroom spines expressing the actin-binding protein Synaptopodin – a marker for spine apparatus - are more prevalent in mutant mice. Previous work identified spines with Synaptopodin/spine apparatus as the locus of mGluR-LTD, which is abnormally elevated in *Fmr1* KO mice. Altogether, our data suggest this enhancement may be linked to the preponderance of this subset of spines in the mutant. Overall, these findings demonstrate the sensitivity and versatility of the optimized methodology by uncovering a novel facet of spine dysgenesis in *Fmr1* KO mice.

Keywords: $DiIC_{18}$, dendritic spines, excitatory synapses, synaptopodin, Fragile X Syndrome, *Fmr1* knockout mouse, hippocampus

1. Introduction

Dendritic spines are the postsynaptic sites of excitatory synapses. These structures allow for the establishment of neural microcircuits, which are in turn refined by spine remodeling or stabilization. Spines display morphological diversity and a high degree of activity-dependent structural/functional plasticity. For example, large mushroom spines with a prominent head are associated with increased synaptic strength and the formation of more stable synapses. In contrast, thin elongated spines with a smaller head are relatively unstable and are readily modified in response to activity [1]. Alterations in spine density, morphology, and size underlie the changes in synaptic connectivity and strength associated with long-term potentiation (LTP) or depression (LTD), the cellular substrates of learning and memory [2]. Notably, variations in spine number and properties have long been linked to neurodevelopmental and neurodegenerative disorders highlighting the importance of studying spine characteristics [3,4].

Excitatory synapses are also highly heterogeneous at the molecular level, the functional implications of which are just beginning to emerge [5–7]. Different synapses can form onto different sub-regions of individual neurons and brain regions depending on the specific molecular components they contain [7,8]. These diverse synapses can also be differentially modified by activity which underlie learning and memory [9–12], behavioral states [13–15], and disease conditions [3,16–21]. The extent of this synaptic heterogeneity is just beginning to be appreciated and presents a unique challenge. Currently, little is known about the physiological remodeling and pathological alterations at individual subsets of synapses, defined by both structural features and molecular makeup [21–23]. Therefore, to begin addressing this question, we optimized a method combining conventional immunofluorescence with the use of the fluorescent dye $DiIC_{18}$ (or DiI) to concurrent visualization of dendritic spine morphology and synaptic protein composition *in vivo*.

$DiIC_{18}$ (1,1'-dioctadecyl-3,3,3',3'-tetramethylindocarbocyanine perchlorate) is a lipid-soluble dye with weak fluorescence until incorporated in the membrane lipid bilayer, where it diffuses at a rate of 0.2-0.6 mm/day in fixed specimens and 6 mm/day in living tissue [24,25]. Once incorporated in the membrane, $DiIC_{18}$ strongly and persistently labels the entire neuron including the dendritic spines [26–28]. Early attempts of combining $DiIC_{18}$ staining with immunolabeling in brain tissue were hampered by the limited compatibility of $DiIC_{18}$ with detergents commonly used for membrane permeabilization during immunolabeling (*e.g.* Triton X-100, saponin). Indeed, such detergents broadly extract membrane lipids inducing leakage and disappearance of $DiIC_{18}$ from finer neurite structures [29]. Interestingly, recent evidence suggests that digitonin – a detergent-like compound that forms a complex with membrane cholesterol – better preserves $DiIC_{18}$ staining while enabling the detection of abundantly expressed proteins including axonal neurofilaments and nuclear antigens [26]. However, there is still limited evidence validating the capacity of $DiIC_{18}$ to be used in combination with immunolabeling to identify specific subsets of spines [30].

Here we optimized and applied a combined $DiIC_{18}$-immunolabeling method to establish an in-depth characterization of the properties of spine synapses in *Fmr1* knockout (KO) mice, a pre-clinical model of Fragile X Syndrome (FXS). FXS is the most common form of inherited intellectual disability, with a high incidence of autism, arising from transcriptional silencing of the X-linked *FMR1* gene [31,32]. We show that hippocampal spine synapses in pyramidal neurons of juvenile *Fmr1* KO mice display an immature profile with an overabundance of thin and branched spines. The overabundance of immature protrusions is accompanied by an overall reduction in the density of mushroom spines, and smaller spine head width, compared to wild types (WT). Surprisingly, despite their overall decreased abundance, we find that a subset of mushroom spines that express the actin-binding protein Synaptopodin [33] - which marks the presence of a spine apparatus (SA)

[34] - are over-represented in mutant mice. Altogether, these observations demonstrate the sensitivity of the optimized $DiIC_{18}$-based method by revealing alterations in a specific subset of mature spine synapses that contain a SA, a novel facet of spine dysgenesis in FXS.

2. Materials and Methods

2.1 Animals

All animal procedures were conducted following protocols approved by the Albert Einstein College of Medicine, in accordance with the Guide for the care and use of laboratory animals by the United States PHS (Ethic Committee Name: IACUC, approval code #00001117, approval date November 22th, 2019). *Fmr1* KO and WT mice (FVB.129P2-*Pde6b*$^{+}$ strain; The Jackson Laboratories, Bar Harbor, ME) were bred in-house. Mice were fed *ad libitum* and housed with a 12 h light/dark cycle. Experiments were carried out in juvenile mice (1 WT female, 2 WT males, 3 Fmr1 KO males) at postnatal day (PND) 22. Experimental mice were generated by crossing heterozygous females with WT males and genotyped using the following oligonucleotides: oligo.1 GTGGTTAGCTAAAGTGAGGATGAT and oligo.2 GTGGGCTCTATGGCTTCTGAGG for KO, oligo.1 and oligo.3 CAGGTTTGTTGGGATTAACAGATC for WT genotype, respectively.

2.2 $DiIC_{18}$ staining

After euthanasia, brains were removed from the skull, washed three times for 5 min in phosphate buffer (PB) at room temperature, and fixed with 4% paraformaldehyde (PFA) overnight at 4°C. Fixed brains were washed three times for 5 min with PB and 150 µm-thick coronal sections were cut with a vibratome (Leica Microsystems, VT1000S). Tissue sections were labeled with $DiIC_{18}$ (Invitrogen, crystals, cat. D3911) as previously described [25, 29]. Briefly, the tissue sections were unfolded with a paintbrush on a glass slide and $DiIC_{18}$ crystals were applied by gently touching the tissue surface with the tip of an 18-gauge needle covered with crystals. The dye was applied onto regions of interest that included the hippocampus and parietal and prefrontal cortex. For the hippocampus, $DiIC_{18}$ was applied with multiple consecutive touches throughout the region in order to dilute the crystals. This procedure prevents the deposition of excess amounts of crystals in one area and results in different labeling intensity throughout the region to allow for visualization of an individual hippocampal neuron more easily. Next, the tissue sections were very gently overlaid with PB to prevent dehydration and incubated for 15 min at room temperature (RT) protected from light, allowing the crystals to settle onto the tissue. The labeled tissue was then transferred to a multi-well plate with additional PB and incubated at 4°C, protected from light, for seven to ten days followed by image acquisition.

2.3 Immunofluorescence

For combined immunofluorescence (2-step protocol), the tissue sections pre-stained with $DiIC_{18}$ for the indicated time were incubated for 30 min at RT with 100 µg/ml digitonin (Sigma Aldrich; cat. D141) dissolved in 3% bovine serum albumin (BSA)/PB. Next, the tissue was incubated with primary antibodies diluted in digitonin solution for 12 h at 4°C and then washed three times for 5 min with PB. Secondary antibodies conjugated to Alexa Fluor 488 were diluted in 3% BSA/PB and applied for 3 h at RT. Tissue sections were

then washed three times for 5 min with PB and mounted with a cover glass using ProLong (Cell Signaling Technology).

2.4 Antibodies

Antibodies used in this study include rabbit anti-Synpo (1:400; Synaptic Systems, RRID:AB_887825), guinea pig anti-Synpo (1:400; Synaptic Systems, RRID:AB_10549419), guinea pig anti-VGluT2 (1:500; Millipore, RRID:AB_1587626), rabbit anti-Synaptoporin (1:200, Proteintech, RRID:AB_2878022). Anti-rabbit and anti-guinea pig secondary antibodies conjugated to Alexa Fluor 488 (1:400) were obtained from Invitrogen.

2.5 Microscopy and image analysis

Images were acquired with a Leica SP5 point-scan confocal microscope mounted with a 63x oil immersion objective (N.A. 1.4) using 3 or 4x zoom-in function. Images at 1024 x 1024 pixel resolution were acquired with scan speed set at 8 and pinhole configured to 1 Airy unit for each channel. Stacks of images were acquired with a 0.5 µm Z step and reconstructed with Fiji [35] using the maximum intensity projection method (MIP) in the Z-stack function. Analysis of dendritic spines and fluorescent signal overlap were conducted blind to genotype on merged 2D Z-stacks using Fiji. Dendrites and dendritic protrusions were outlined and measured with the segmented line tool. Spine density is expressed as the number of spines per dendritic length (in µm). Morphometric analysis of spine properties was carried out as previously described [30]. Briefly, the length (l), head (h) and neck (n) width of dendritic protrusions were manually traced. The length was measured from the edge of the dendritic shaft to the tip of the protrusions; head dimensions were measured at the point of maximum width. Dendritic protrusions were classified according to commonly accepted criteria as described previously [30], including mushroom spines ($h \gg n$, $h/n > 1.5$), thin spines ($l > 1$ µm, $h/n < 1.5$), stubby spines ($l < 0.5$ µm, $h/n \leq 1$), filopodia ($h = n$; $l > 3$ µm, $0.1 < n < 0.4$ µm) and branched cup-shaped spines (neck split into 2 sub-necks, each with a small head). To quantify Synaptopodin-positive (*S*+) and Synaptopodin-negative (*S*-) spines, a color-merged image of $DiIC_{18}$ and Synaptopodin signal was generated, and spines were counted with the Cell Counter plugin. Points of fluorescent signal overlap were identified with the Colocalization Threshold and Coloc2 plugins after background subtraction and quantified with the Cell counter tool.

2.6 Statistical analysis

Data are reported as mean ± SEM; comparisons between two groups used unpaired *t*-test with Welch's correction. Generation of graphs and statistical tests were carried out with Prism 8.1 (GraphPad).

3. Results

3.1 $DiIC_{18}$ combined with immunolabeling enables morphological and molecular characterization of individual spine synapses

In the past, $DiIC_{18}$ has been successfully used for neuron tracing due to its ability to become incorporated into the plasma membrane and diffuse throughout the entire neuron [36–39]. In 2008, Matsubayashi and colleagues explored the possibility of combining $DiIC_{18}$ staining with immunodetection of abundant cytoskeletal and nuclear antigens using digitonin to improve antibody penetration into brain tissue without substantial loss of

$DiIC_{18}$ signal [26]. Here, we report a simple and reliable optimized method to visualize individual spine synapses and low abundance synaptic proteins in brain tissue using $DiIC_{18}$ staining in combination with immunofluorescence and high-resolution confocal microscopy. The method includes either a simple 1-step protocol limited to visualization of neurites, or a 2-step protocol for combined detection of post- or pre-synaptic proteins (Figure 1). In the 1-step protocol, mouse brain tissue sections are incubated with $DiIC_{18}$ for seven to ten days followed by the acquisition of image stacks by confocal microscopy (Figure 1a). Dendritic protrusions are well preserved and can be outlined and measured using Fiji, an open-source image-processing platform [35]. The density of dendritic protrusions of different morphology, alterations of which is a hallmark of neurodevelopmental and neurodegenerative disorders, can be determined by classification according to established morphologic criteria (for details see *Material and Methods*). In the 2-step protocol, brain tissue sections are first stained with $DiIC_{18}$ for seven to ten days, then permeabilized with digitonin (100 µg/ml) and immunolabeled in a digitonin solution containing primary antibodies (Figure 1b) followed by incubation with appropriate fluorescent secondary antibodies in a 3% BSA/PB solution (for details see *Material and Methods*). The structural integrity of dendritic spines and membrane incorporation of $DiIC_{18}$ are maintained after incubation with digitonin, as illustrated by the visualization of a subset of mushroom spines that express Synaptopodin, a marker of the SA (Figure 1b).

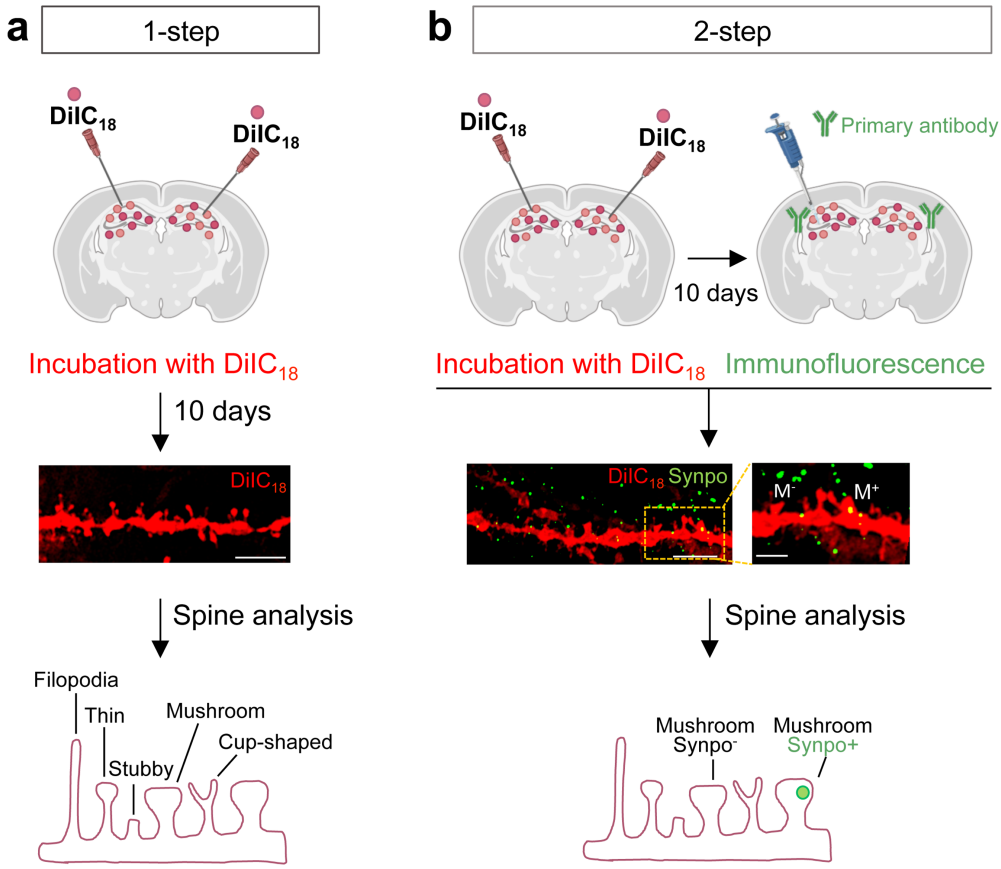

Figure 1. Workflow of $DiIC_{18}$ staining combined with fluorescent immunolabeling. (a) Overview of the 1-step protocol for visualization and morphometric analysis of dendritic spines in rodent brain tissue. Shown in the middle panel is a representative confocal image of an area of the hippocampus from a coronal section of WT mouse brain stained with $DiIC_{18}$; scale bar, 5 µm. Bottom panel, graphical representation of different

types of dendritic spines. (b) Overview of a 2-step protocol for morphometric analysis combined with detection of synaptic proteins. Shown in the middle panel is a representative confocal image of an area of the hippocampus from a coronal section stained with $DiIC_{18}$ and immunolabeled with anti-Synaptopodin (Synpo) antibody: scale bar 5 µm, magnified inset 2 µm. M-, Synpo-negative mushroom spine; M+ Synpo-positive mushroom spine. Illustrations in the top panels of (a) and (b) were created with Biorender.com.

The 2-step protocol can be applied to visualize presynaptic sites expressing different subsets of proteins, thus distinguishing individual synapses based on both morphological and molecular identity and allowing one to access the complexity and heterogeneity of synapses in the brain. Using this method we were successfully able to visualize a subset of dendritic spines with different microanatomy – presence *vs.* absence of a SA labeled with anti-Synaptopodin – adjacent to presynaptic terminals expressing either Vesicular Glutamate Transporter 2 (VGluT2; Figure 2a,b) or Synaptoporin (Synpr; Figure 2a,b) enriched in hippocampal mossy fibers [40].

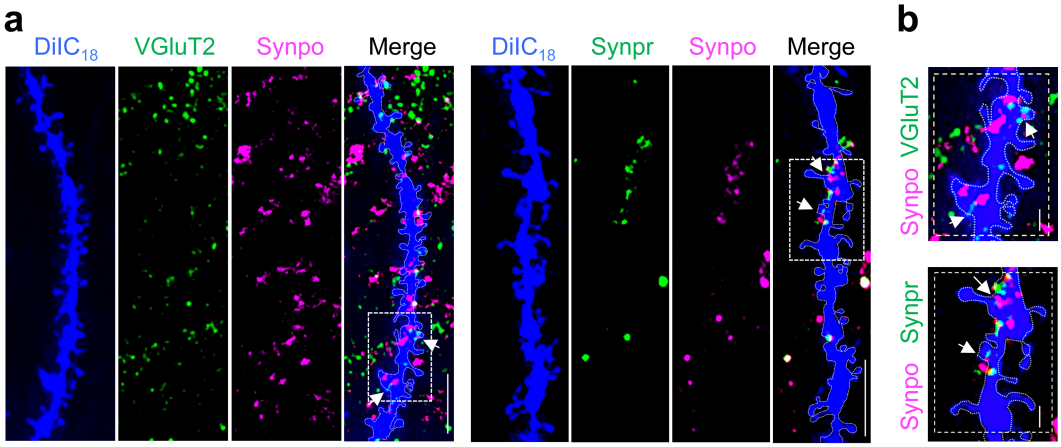

Figure 2. Visualization of Synpo-containing spines and VGluT2- or Synpr-positive terminals at hippocampal synapses *in vivo*. (a) Representative confocal images of WT hippocampal dendrites stained with $DiIC_{18}$ and labeled with anti-Synaptopodin (Synpo) together with either anti-VGluT2 (left panels) or anti-Synpr (right panels). Shown are individual channels ($DiIC_{18}$ in blue) and the overlay of the three-channels (Merge); boxed areas are shown magnified in (b), scale bars 5 µm. (b) Magnified images of boxed areas in (a); scale bars, 2 µm. Arrows point to regions of Synpo/VGluT2 or Synpo/Synpr overlap.

Altogether, these examples demonstrate the sensitivity and resolution afforded by combining $DiIC_{18}$ staining with immunofluorescence for the characterization of excitatory synapses in native tissue.

3.2 Dysgenesis of dendritic spines in the hippocampus of juvenile Fmr1 KO mice

Abnormalities in the density and morphology of dendritic spines have been linked to dysfunctions in neuronal networks in neurodevelopmental disorders, including FXS [41–43]. Early studies in FXS patients indicated an overabundance of spines [44], however, analysis of *Fmr1* KO mice has produced conflicting results, in particular in the hippocampal region [45]. In the mature (> 60 PND) hippocampus of *Fmr1* KO mice, either increased density of dendritic protrusions [46], normal density [47], or subregion-specific differences were noted compared to WT [48].

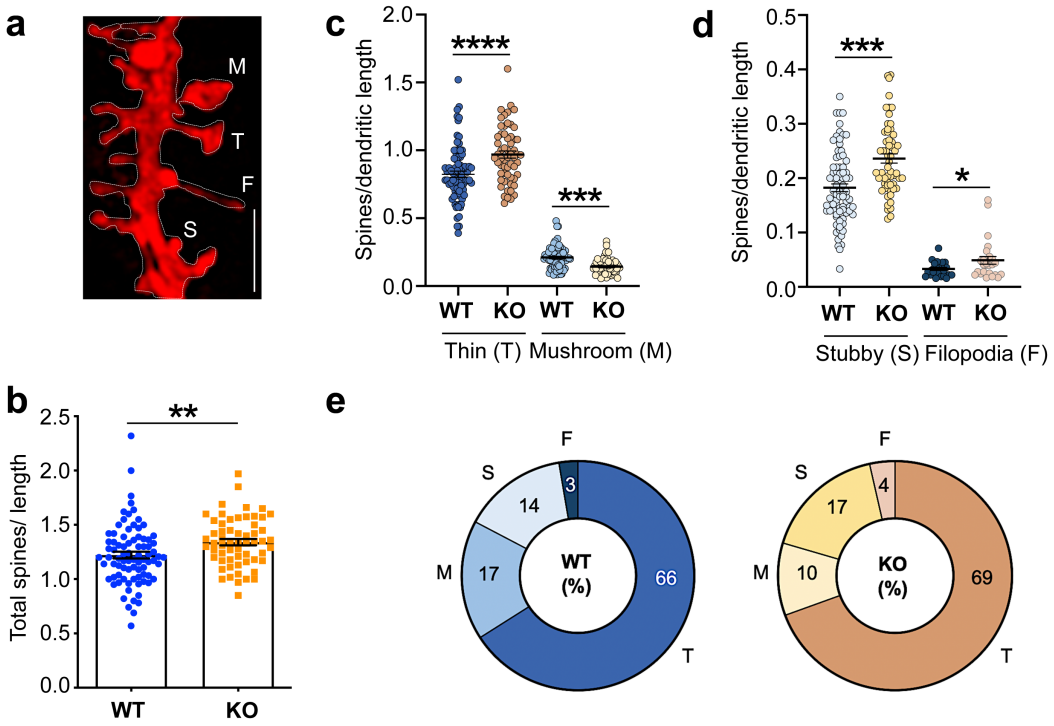

Figure 3. DiIC$_{18}$ staining reveals dysgenesis of hippocampal spines in juvenile *Fmr1* KO mice. (a) Representative confocal image of a dendritic segment from WT mouse hippocampus stained with DiIC$_{18}$; scale bar, 2 µm. Labels indicate the different types of dendritic protrusions identified: M mushroom spines, T thin spines, S stubby spines, F filopodia. (b) Quantification of total dendritic protrusions per dendritic length (µm) in WT and *Fmr1* KO mice. (c-d) Quantification of the density of spines categorized by morphology including (c) thin and mushroom spines and (d) stubby spines and filopodia. (e) Pie charts reporting the relative proportion (%) of the four most common types of spines observed in hippocampal pyramidal neurons in juvenile WT and *Fmr1* KO mice.

Here, we used combined DiIC$_{18}$ staining and immunofluorescence to examine the properties of excitatory spine synapses in the hippocampus of *Fmr1* KO mice at PND22, when the main wave of synaptogenesis is concluded ([49]). Spine properties were evaluated in CA1 and CA3 pyramidal neurons by quantitative analysis of high-resolution confocal images that enable visualization of fine morphological features (Figure 3a). Spine density was first calculated by considering the total number of protrusions per length of dendritic segment, regardless of morphology. Concordant with findings in the adult hippocampus [46], we found that the overall density of dendritic protrusions was higher in *Fmr1* KO mice compared to WT (Figure 3b; protrusions/µm mean ± SEM, WT 1.22 ± 0.031 n = 82 dendrites *vs*. *Fmr1* KO 1.34 ± 0.029 n = 59 from N = 3 mice per group; $p = 0.006$). Next, we evaluated dendritic spine maturation determined based on morphological features including length, head width, and presence of a discernible neck region (see *Material and Methods* for details). The density of thin spines (spines/µm mean ± SEM, WT 0.82 ± 0.14 n = 82 *vs*. *Fmr1* KO 0.97 ± 0.035 n = 59; $p < 0.0001$), stubby spines (mean ± SEM, WT 0.18 ± 0.007 n = 82 *vs.* Fmr1 KO 0.24 ± 0.008 n = 59; $p < 0.0001$) and filopodia (mean ± SEM, WT 0.03 ± 0.003 n = 25 *vs. Fmr1* KO 0.05 ± 0.007 n = 26; $p = 0.046$) was uniformly higher in the *Fmr1* KO compared to WT (Figure 3c,d). In contrast, mushroom spines were significantly less abundant in the mutant (Figure 3c; mean ± SEM, WT 0.21 ± 0.009 n = 82 *vs. Fmr1* KO 0.14 ± 0.007 n = 59, $p < 0.0001$), representing ~ 10% of all dendritic protrusions compared to ~ 17% in WT (Figure 3e).

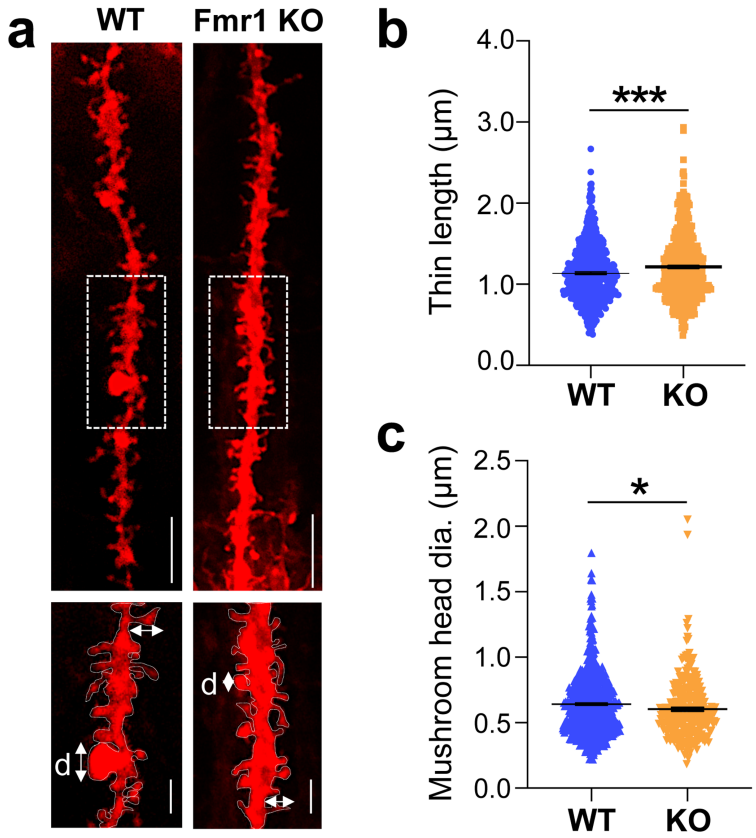

Figure 4. Morphological alterations of thin and mushroom spines in the *Fmr1* KO mouse hippocampus. (a) Representative confocal images of dendritic branches stained with $DiIC_{18}$ from WT and *Fmr1* KO hippocampi; scale bars, 5 µm. Boxed regions are displayed in magnified insets below; scale bars, 2 µm. Arrows indicate the length and head width measurements; d, diameter of spine heads. (b) Quantification of the length of thin spines in WT and *Fmr1* KO littermates. (c) Quantification of mushroom spines head width (diameter) in WT and *Fmr1* KO mice.

Previous analysis of cortical and hippocampal regions in adult *Fmr1* KO mice using Golgi staining identified a prevalence of elongated and tortuous spines deemed 'immature' in appearance [47,50]. To assess morphological spine properties in the hippocampus of juvenile mutant mice, we measured the length and head width of individual protrusions in high-resolution images of $DiIC_{18}$-stained tissue (Figure 4a). In *Fmr1* KO mice, thin spines appeared significantly more elongated than in WT littermates (Figure 4b; WT 1.13 ± 0.023, n = 569 spines, *Fmr1* KO 1.21 ± 0.079 n = 480; $p < 0.0009$) whereas the head width of mushroom spines was comparatively smaller (Figure 4c; WT 0.64 ± 0.016 n = 690, *Fmr1* KO 0.60 ± 0.039 n = 276; $p = 0.018$). High-resolution imaging also enabled the visualization of an additional category of spines characterized by a cup-shaped head (Figure 5a), termed cup-shaped or branched spines [51]. Although relatively sparse, branched spines were observed more frequently in *Fmr1* KO mice compared to WT littermates (Figure 5b; spines/µm WT 0.003 ± 0.001, n = 69 dendrites, *Fmr1* KO 0.012 ± 0.003 n = 60; $p = 0.0043$) and were detected in ~ 28% of the dendritic branches examined compared to ~ 10% in WT (Figure 5c).

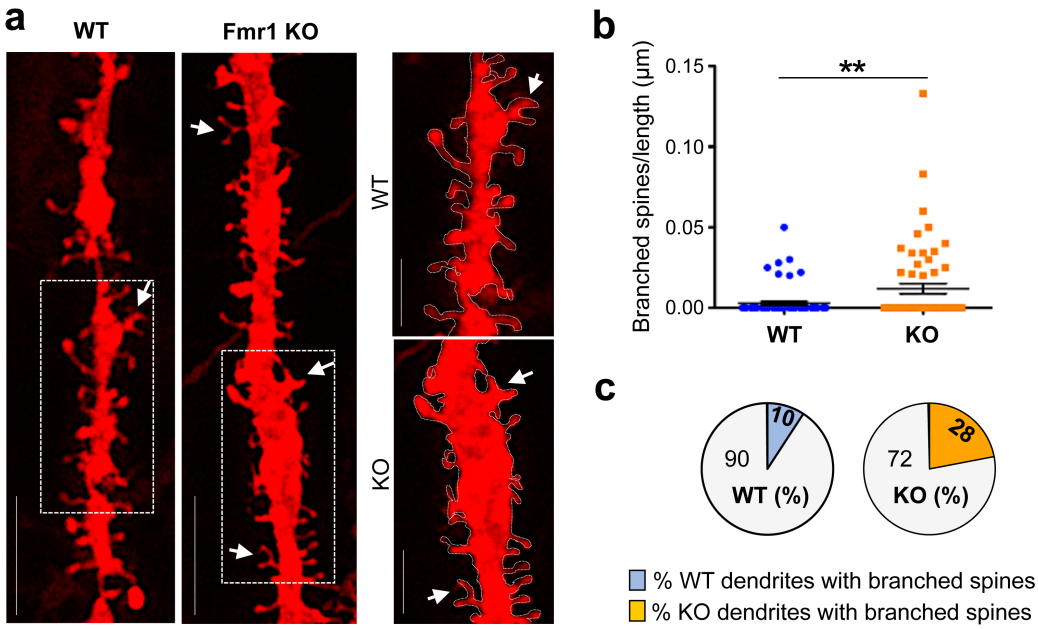

Figure 5. Abnormal prevalence of branched spines in the hippocampus of juvenile *Fmr1* KO mice. (a) Representative confocal images of dendritic branches stained with $DiIC_{18}$ from WT and *Fmr1* KO hippocampi; scale bars, 5 µm. Boxed regions are displayed in magnified insets (right panels), scale bars, 2 µm. Arrows point to branched, cup-shaped spines. (b) Quantification of the relative density of branched (cup-shaped) spines per neurite length (µm) in WT and *Fmr1* KO mice. (c) Pie charts report the relative proportion (%) of dendrites with branched spines relative to all dendritic branches examined.

Thus, at the completion of synaptogenesis and prior to potential compensatory changes in adulthood, the hippocampus of juvenile *Fmr1* KO mice displays an overall increased density of dendritic protrusions. This abnormality is further compounded by pervasive spine dysgenesis, exemplified by the prevalence of elongated thin spines and branched spines and concomitant with depletion of mushroom spines.

3.3 Surplus of mushroom spines expressing Synpo in the hippocampus of Fmr1 KO mice.

Mature mushroom spines of telencephalic regions are characterized by heterogeneous microanatomy, with ~ 20% harboring a SA. The SA is composed of folded smooth ER tubules intercalated by actin filaments and Synpo, an actin-binding protein that is required for the formation and maintenance of the SA [34]. The formation of a SA in the postnatal brain follows the developmentally regulated expression of Synpo protein, first detected at ~ PND5 and reaching adult levels at ~ PND20 [52,53]. Mushroom spines with Synpo/SA have higher synaptic strength [54] and longer lifetime than those in which Synpo/SA is absent [33].

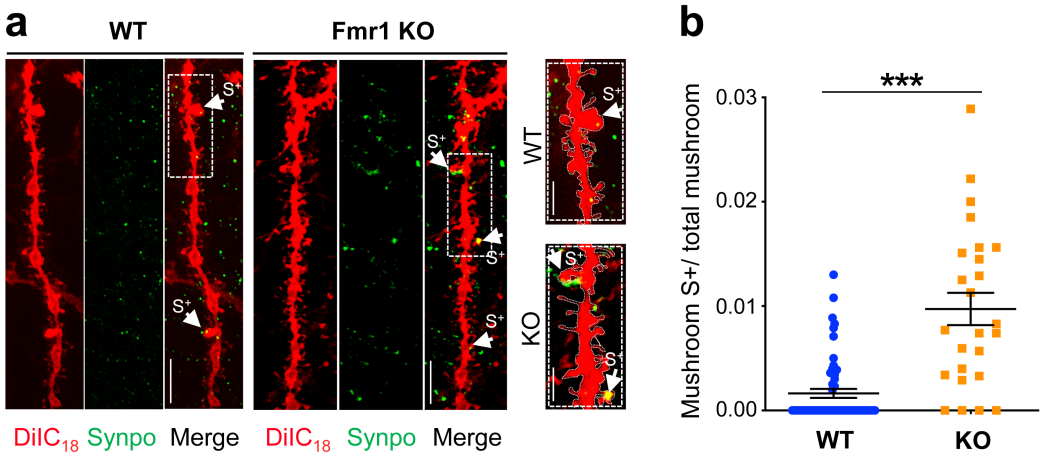

Figure 6. Increased abundance of mushroom spines containing Synpo in juvenile *Fmr1* KO mice. (a) Representative confocal images of dendritic branches stained with $DiIC_{18}$ and immunolabeled with anti-Synpo from WT and *Fmr1* KO hippocampi; scale bars, 5 µm. Boxed areas are shown magnified in insets (right panels), scale bars 2 µm. Arrows point to Synpo-positive (S+) mushroom spines. (b) Quantification of Synpo-positive (S+) mushroom spines relative to the total number of mushroom spines in WT and *Fmr1* KO mice.

Although only partly understood, a function of the SA is local regulation of calcium [55]. Moreover, the presence of Synpo/SA in spines was recently shown to be required for induction of group I mGluR-dependent long-term depression (mGluR-LTD) at hippocampal synapses [30]. Since abnormally enhanced mGluR-LTD [56,57] is an established phenotype of *Fmr1* KO mice, we applied $DiIC_{18}$ staining in combination with immunolabeling with anti-Synpo (2-step protocol; Figure 1b) to examine the abundance of spines expressing Synpo/SA in the *Fmr1* KO hippocampus at PND22, when Synpo expression has stabilized (Figure 6a). Notably, we found that the relative abundance of Synpo-positive (S+) mushroom spines compared to total mushroom spines (Figure 6b; WT 0.002 ± 0.0004 n = 55, *Fmr1* KO 0.010 ± 0.0015 n = 25, $p < 0.0001$) was higher in *Fmr1* KO mice compared to WT. Thus, although juvenile *Fmr1* KO mice display a prevalence of immature spines and overall reduced density of mushroom spines, stable mushroom spines containing Synpo/SA are over-represented compared to WT.

4. Discussion

Alteration of excitatory spine synapses is a hallmark of neurodevelopmental disorders including FXS, autism, and schizophrenia as well as of neurodegenerative disorders [3,4]. Here, we describe a sensitive method to facilitate rapid, in-depth investigation of the properties of spine synapses in brain tissue. The method, relying on the combined use of the fluorescent dye $DiIC_{18}$ and optimized conditions for *in situ* detection of low abundance synaptic proteins, offers several advantages. First, it enables precise morphometric analysis of finer dendritic protrusions with complex morphology (*e.g.,* branched spines). Second, the concurrent visualization of structural landmarks and protein expression/localization permits the identification of individual subsets of excitatory synapses (*e.g.,* spines containing the SA) which can be distinguished from one another and allow one to begin to dissect the vast heterogeneity of the intact brain. Third, the approach is versatile and can be applied to any brain region and any animal model, independent of genetically encoded fluorescent reporters. Finally, and importantly, it can be used on fixed tissue sections that can be stored prior to labeling, thus providing an extended time window for analysis, crucial for translating experiments and results to human tissue.

In this paper we successfully demonstrate the sensitivity and applicability of this approach by completing an in-depth characterization of spine synapses in the hippocampus of *Fmr1* KO mice, an animal model of FXS [58]. FXS is caused by a CGG expansion in the 5'-UTR of the *FMR1* gene, resulting in transcriptional silencing and downregulation/loss of the encoded FMRP protein [59]. FXS is part of a group of brain disorders termed 'synaptopathies' thought to arise from dysfunctions of synapse development and plasticity [42,60–64]. An overabundance of spines with immature morphology was observed in cortical and hippocampal regions of FXS patients [42,65] suggesting defects in excitatory synapse formation/maintenance. The *Fmr1* KO mouse recapitulates many manifestations of FXS and has been instrumental in understanding its molecular and cellular underpinnings. However, studies of spine dysgenesis in mutant mice have remained inconclusive [42,44,45,66] with reports of either overabundance of spines with immature morphology or lack of detectable alterations [45]. Such discrepancy, particularly notable in the hippocampus, was attributed to differences in methodology (Golgi staining *vs. in vivo* live imaging), brain area, and/or age under consideration.

In this study, we used the optimized labeling method to re-examine the properties of excitatory spine synapses in the *Fmr1* KO hippocampus at PND22 (juvenile). This age was chosen because it is past the hippocampal critical period of plasticity, the main wave of synaptogenesis is concluded [48], and hippocampal-based memories can form [67]. We detected an overabundance of thin spines that also appeared abnormally elongated in the dendrites of pyramidal neurons of mutant mice. These alterations, suggestive of an *immature* state, are concordant with reports in FXS patients and several reports in cortical regions of the *Fmr1* KO mouse. Moreover, we found that mutant mice display an excessive number of branched cup-shaped spines compared to WT, an abnormality not previously noted. In the rat hippocampus, cup-shaped spines are rare at PND15 but more frequent in the adult [68], and their density increases in response to stimulation such as environmental enrichment and LTP [69–71]. Branched spines were mostly described in studies using reconstructions from electron microscopy images and are seldom considered in morphological analyses by Golgi staining or *in vivo* 2-photon imaging, likely due to limited resolution. With the advent of super-resolution microscopy, branched spines were shown to be dynamic [72] and endowed with complex organization of the actin cytoskeleton [73]. Individual branches of cup-shaped spines were reported to receive inputs from separate boutons [69,74]. Interestingly, multiple innervation of spines was recently shown to occur in the somatosensory cortex of PND10-15 *Fmr1* KO mice and linked to circuit hyperexcitability [75]. Although untested, it is possible that an increased abundance of branched spines in the juvenile hippocampus may be linked to the hyperexcitable network in mutant mice [76,77].

Concomitant to an overabundance of thin and branched spines, we detected a decreased abundance of mushroom spines that also displayed smaller heads than WT. Mushroom spines form strong synapses, as indicated by the correlation of head dimensions with higher synaptic strength and AMPA receptor content [78]. Such spine synapses are stable and were shown in some cases to endure for weeks to potentially organismal lifetime. In particular, mushroom spines containing the SA were shown to be more stable, with longer lifetime [33] and higher synaptic strength [54] than those without. Unexpectedly, we found that mushroom spines with SA are more represented in hippocampal pyramidal neurons of *Fmr1* KO mice than in WT. This observation is concordant with findings in organotypic slice cultures in which thorny excrescences, the postsynaptic locus of DG mossy fiber boutons-CA3 synapses, show augmented formation of the SA in *Fmr1* KO mice as determined by Synpo labeling [77]. Mushroom spines containing the SA are required for induction of mGluR-LTD at CA3-CA1 synapses, a form of plasticity that is abnormally enhanced in *Fmr1* KO mice [30,56,79,80]. Moreover, mGluR-LTD was found to induce loss of mushroom spines that do not contain a SA while sparing those in which the SA is present [30]. The enhanced density of mushroom spines with SA in *Fmr1* KO mice

would be in line with mGluR-LTD enhancement and overall reduced abundance of mushroom spines in the mutant. Future experiments will determine whether overabundance of SA-containing spines is causally related to, and potentially precedes, abnormal mGluR-LTD in the mutant.

5. Conclusions

We report the development of an optimized methodology to investigate the morphological and molecular properties of excitatory spines synapses in brain tissue. The feasibility and advantages of the methodology are supported by the demonstration of its capacity to identify abnormalities in morphology and composition of spine synapses in a mouse model of Fragile X syndrome. Amongst the observed defects, we detail the previously undetected prevalence of spines containing a spine apparatus that may be linked to aberrant synaptic plasticity in mutant mice.

Author Contributions: conceptualization, L.S., A.F.; methodology, L.S.; validation, L.S., F.V., A.F.; formal analysis, L.S., A.F., F.V., S.P. investigation, L.S., K.D.F., S.G.; resources, A.F.; data curation, L.S.; writing—original draft preparation, L.S., F.V., A.F.; writing—review and editing, L.S., S.G., C.P.C., F.V., A.F.; visualization, L.S., A.F.; supervision, C.P.C., F.V., A.F.; project administration, F.V., A.F.; funding acquisition, A.F. All authors have read and agreed to the published version of the manuscript.

Funding: National Institutes of Health MH108614 (A.F.); POR Campania FESR 2014/2020" (Project N. B61G18000470007) from Regione Campania, Italy (C.P.C), Progetto 000005_2018_RARE.PLAT.NET and 000005_BUDGET_ECONOMICO_RICERCA_2020 (F.V).

Acknowledgments: We acknowledge the assistance of the Neural Cell Engineering and Imaging Core of the Einstein Rose F. Kennedy Intellectual and Developmental Disabilities Research Center supported by the National Institute of Child Health and Human Development U54 HD090260, and of the Analytical Imaging Facility at Albert Einstein College of Medicine partly funded by National Cancer Institute Cancer Center Grant P30CA013330.

References

1. Bourne, J.; Harris, K.M. Do Thin Spines Learn to Be Mushroom Spines That Remember? *Current Opinion in Neurobiology* **2007**, *17*, 381–386, doi:10.1016/j.conb.2007.04.009.
2. Segal, M. Dendritic Spines: Morphological Building Blocks of Memory. *Neurobiology of Learning and Memory* **2017**, *138*, 3–9, doi:10.1016/j.nlm.2016.06.007.
3. Penzes, P.; Cahill, M.E.; Jones, K.A.; VanLeeuwen, J.-E.; Woolfrey, K.M. Dendritic Spine Pathology in Neuropsychiatric Disorders. *Nat. Neurosci.* **2011**, *14*, 285–293, doi:10.1038/nn.2741.
4. Penzes, P.; Buonanno, A.; Passafaro, M.; Sala, C.; Sweet, R.A. Developmental Vulnerability of Synapses and Circuits Associated with Neuropsychiatric Disorders. *J. Neurochem.* **2013**, *126*, 165–182, doi:10.1111/jnc.12261.
5. Berry, K.P.; Nedivi, E. Spine Dynamics: Are They All the Same? *Neuron* **2017**, *96*, 43–55, doi:10.1016/j.neuron.2017.08.008.

6. Grant, S.G.N.; Fransén, E. The Synapse Diversity Dilemma: Molecular Heterogeneity Confounds Studies of Synapse Function. *Front. Synaptic Neurosci.* **2020**, *12*, 590403, doi:10.3389/fnsyn.2020.590403.
7. Helm, M.S.; Dankovich, T.M.; Mandad, S.; Rammner, B.; Jähne, S.; Salimi, V.; Koerbs, C.; Leibrandt, R.; Urlaub, H.; Schikorski, T.; et al. A Large-Scale Nanoscopy and Biochemistry Analysis of Postsynaptic Dendritic Spines. *Nat Neurosci* **2021**, *24*, 1151–1162, doi:10.1038/s41593-021-00874-w.
8. Cizeron, M.; Qiu, Z.; Koniaris, B.; Gokhale, R.; Komiyama, N.H.; Fransén, E.; Grant, S.G.N. A Brain-wide Atlas of Synapses across the Mouse Life Span. *Science* **2020**, *369*, 270–275, doi:10.1126/science.aba3163.
9. Danielson, E.; Perez de Arce, K.; Cimini, B.; Wamhoff, E.-C.; Singh, S.; Cottrell, J.R.; Carpenter, A.E.; Bathe, M. Molecular Diversity of Glutamatergic and GABAergic Synapses from Multiplexed Fluorescence Imaging. *eNeuro* **2021**, *8*, ENEURO.0286-20.2020, doi:10.1523/ENEURO.0286-20.2020.
10. Venkatesan, S.; Subramaniam, S.; Rajeev, P.; Chopra, Y.; Jose, M.; Nair, D. Differential Scaling of Synaptic Molecules within Functional Zones of an Excitatory Synapse during Homeostatic Plasticity. *eNeuro* **2020**, *7*, ENEURO.0407-19.2020, doi:10.1523/ENEURO.0407-19.2020.
11. Ma, L.; Qiao, Q.; Tsai, J.-W.; Yang, G.; Li, W.; Gan, W.-B. Experience-Dependent Plasticity of Dendritic Spines of Layer 2/3 Pyramidal Neurons in the Mouse Cortex: Experience-Dependent Dendritic Spine Remodeling. *Devel Neurobio* **2016**, *76*, 277–286, doi:10.1002/dneu.22313.
12. Pignataro, A.; Ammassari-Teule, M. Post-Extinction Selective Persistence of Large Dendritic Spines in Fear Remodeled Circuits May Serve to Reactivate Fear. *Current Opinion in Neurobiology* **2015**, *35*, 1–5, doi:10.1016/j.conb.2015.04.005.
13. Gisabella, B.; Scammell, T.; Bandaru, S.S.; Saper, C.B. Regulation of Hippocampal Dendritic Spines Following Sleep Deprivation. *J Comp Neurol* **2020**, *528*, 380–388, doi:10.1002/cne.24764.
14. Zhou, Y.; Lai, C.S.W.; Bai, Y.; Li, W.; Zhao, R.; Yang, G.; Frank, M.G.; Gan, W.-B. REM Sleep Promotes Experience-Dependent Dendritic Spine Elimination in the Mouse Cortex. *Nat Commun* **2020**, *11*, 4819, doi:10.1038/s41467-020-18592-5.
15. de Vivo, L.; Bellesi, M.; Marshall, W.; Bushong, E.A.; Ellisman, M.H.; Tononi, G.; Cirelli, C. Ultrastructural Evidence for Synaptic Scaling across the Wake/Sleep Cycle. *Science* **2017**, *355*, 507–510, doi:10.1126/science.aah5982.
16. Grant, S.G.N. Synapse Diversity and Synaptome Architecture in Human Genetic Disorders. *Human Molecular Genetics* **2019**, *28*, R219–R225, doi:10.1093/hmg/ddz178.
17. Phillips, M.; Pozzo-Miller, L. Dendritic Spine Dysgenesis in Autism Related Disorders. *Neuroscience Letters* **2015**, *601*, 30–40, doi:10.1016/j.neulet.2015.01.011.
18. Hoover, B.R.; Reed, M.N.; Su, J.; Penrod, R.D.; Kotilinek, L.A.; Grant, M.K.; Pitstick, R.; Carlson, G.A.; Lanier, L.M.; Yuan, L.-L.; et al. Tau Mislocalization to Dendritic Spines Mediates Synaptic Dysfunction Independently of Neurodegeneration. *Neuron* **2010**, *68*, 1067–1081, doi:10.1016/j.neuron.2010.11.030.
19. Pekala, M.; Doliwa, M.; Kalita, K. Impact of Maternal Immune Activation on Dendritic Spine Development. *Develop. Neurobiol.* **2021**, *81*, 524–545, doi:10.1002/dneu.22804.
20. Dorostkar, M.M.; Zou, C.; Blazquez-Llorca, L.; Herms, J. Analyzing Dendritic Spine Pathology in Alzheimer's Disease: Problems and Opportunities. *Acta Neuropathol* **2015**, *130*, 1–19, doi:10.1007/s00401-015-1449-5.
21. Wang, G.X.; Smith, S.J.; Mourrain, P. Fmr1 KO and Fenobam Treatment Differentially Impact Distinct Synapse Populations of Mouse Neocortex. *Neuron* **2014**, *84*, 1273–1286, doi:10.1016/j.neuron.2014.11.016.
22. Shao, L.-X.; Liao, C.; Gregg, I.; Davoudian, P.A.; Savalia, N.K.; Delagarza, K.; Kwan, A.C. Psilocybin

Induces Rapid and Persistent Growth of Dendritic Spines in Frontal Cortex in Vivo. *Neuron* **2021**, *109*, 2535-2544.e4, doi:10.1016/j.neuron.2021.06.008.

23. Phoumthipphavong, V.; Barthas, F.; Hassett, S.; Kwan, A.C. Longitudinal Effects of Ketamine on Dendritic Architecture *In Vivo* in the Mouse Medial Frontal Cortex. *eNeuro* **2016**, *3*, ENEURO.0133-15.2016, doi:10.1523/ENEURO.0133-15.2016.

24. Staffend, N.A.; Meisel, R.L. DiOlistic Labeling of Neurons in Tissue Slices: A Qualitative and Quantitative Analysis of Methodological Variations. *Front. Neuroanat.* **2011**, *5*, doi:10.3389/fnana.2011.00014.

25. Cheng, C.; Trzcinski, O.; Doering, L.C. Fluorescent Labeling of Dendritic Spines in Cell Cultures with the Carbocyanine Dye "DiI." *Front Neuroanat* **2014**, *8*, 30, doi:10.3389/fnana.2014.00030.

26. Matsubayashi, Y.; Iwai, L.; Kawasaki, H. Fluorescent Double-Labeling with Carbocyanine Neuronal Tracing and Immunohistochemistry Using a Cholesterol-Specific Detergent Digitonin. *Journal of Neuroscience Methods* **2008**, *174*, 71–81, doi:10.1016/j.jneumeth.2008.07.003.

27. Trivino-Paredes, J.S.; Nahirney, P.C.; Pinar, C.; Grandes, P.; Christie, B.R. Acute Slice Preparation for Electrophysiology Increases Spine Numbers Equivalently in the Male and Female Juvenile Hippocampus: A DiI Labeling Study. *Journal of Neurophysiology* **2019**, *122*, 958–969, doi:10.1152/jn.00332.2019.

28. Viggiano, D.; Speranza, L.; Crispino, M.; Bellenchi, G.C.; di Porzio, U.; Iemolo, A.; De Leonibus, E.; Volpicelli, F.; Perrone-Capano, C. Information Content of Dendritic Spines after Motor Learning. *Behav Brain Res* **2018**, *336*, 256–260, doi:10.1016/j.bbr.2017.09.020.

29. Elberger, A.J.; Honig, M.G. Double-Labeling of Tissue Containing the Carbocyanine Dye DiI for Immunocytochemistry. *J Histochem Cytochem.* **1990**, *38*, 735–739, doi:10.1177/38.5.2110209.

30. Speranza, L.; Inglebert, Y.; De Sanctis, C.; Wu, P.Y.; Kalinowska, M.; McKinney, R.A.; Francesconi, A. Stabilization of Spine Synaptopodin by MGluR1 Is Required for MGluR-LTD. *J. Neurosci.* **2022**, *42*, 1666–1678, doi:10.1523/JNEUROSCI.1466-21.2022.

31. Hagerman, R.J.; Berry-Kravis, E.; Hazlett, H.C.; Bailey, D.B.; Moine, H.; Kooy, R.F.; Tassone, F.; Gantois, I.; Sonenberg, N.; Mandel, J.L.; et al. Fragile X Syndrome. *Nat Rev Dis Primers* **2017**, *3*, 17065, doi:10.1038/nrdp.2017.65.

32. Nobile, V.; Pucci, C.; Chiurazzi, P.; Neri, G.; Tabolacci, E. DNA Methylation, Mechanisms of FMR1 Inactivation and Therapeutic Perspectives for Fragile X Syndrome. *Biomolecules* **2021**, *11*, 296, doi:10.3390/biom11020296.

33. Yap, K.; Drakew, A.; Smilovic, D.; Rietsche, M.; Paul, M.H.; Vuksic, M.; Del Turco, D.; Deller, T. The Actin-Modulating Protein Synaptopodin Mediates Long-Term Survival of Dendritic Spines. *eLife* **2020**, *9*, e62944, doi:10.7554/eLife.62944.

34. Deller, T.; Korte, M.; Chabanis, S.; Drakew, A.; Schwegler, H.; Stefani, G.G.; Zuniga, A.; Schwarz, K.; Bonhoeffer, T.; Zeller, R.; et al. Synaptopodin-Deficient Mice Lack a Spine Apparatus and Show Deficits in Synaptic Plasticity. *Proc. Natl. Acad. Sci. U.S.A.* **2003**, *100*, 10494–10499, doi:10.1073/pnas.1832384100.

35. Schindelin, J.; Arganda-Carreras, I.; Frise, E.; Kaynig, V.; Longair, M.; Pietzsch, T.; Preibisch, S.; Rueden, C.; Saalfeld, S.; Schmid, B.; et al. Fiji: An Open-Source Platform for Biological-Image Analysis. *Nat Methods* **2012**, *9*, 676–682, doi:10.1038/nmeth.2019.

36. Honig, M.G.; Hume, R.I. Fluorescent Carbocyanine Dyes Allow Living Neurons of Identified Origin to Be Studied in Long-Term Cultures. *Journal of Cell Biology* **1986**, *103*, 171–187, doi:10.1083/jcb.103.1.171.

37. Honig, M.G.; Hume, R.I. Dil and DiO: Versatile Fluorescent Dyes for Neuronal Labelling and Pathway Tracing. *Trends Neurosci* **1989**, *12*, 333–335, 340–341.

38. Sparks, D.L.; Lue, L.-F.; Martin, T.A.; Rogers, J. Neural Tract Tracing Using Di-I: A Review and a New

Method to Make Fast Di-I Faster in Human Brain. *Journal of Neuroscience Methods* **2000**, *103*, 3–10, doi:10.1016/S0165-0270(00)00291-0.

39. Vercelli, A.; Repici, M.; Garbossa, D.; Grimaldi, A. Recent Techniques for Tracing Pathways in the Central Nervous System of Developing and Adult Mammals. *Brain Research Bulletin* **2000**, *51*, 11–28, doi:10.1016/S0361-9230(99)00229-4.

40. Woelfle, S.; Boeckers, T.M. Layer-Specific Vesicular Glutamate Transporter 1 Immunofluorescence Levels Delineate All Layers of the Human Hippocampus Including the Stratum Lucidum. *Front. Cell. Neurosci.* **2021**, *15*, 789903, doi:10.3389/fncel.2021.789903.

41. Martínez-Cerdeño, V. Dendrite and Spine Modifications in Autism and Related Neurodevelopmental Disorders in Patients and Animal Models: Dendrite and Spine in Autism. *Devel Neurobio* **2017**, *77*, 393–404, doi:10.1002/dneu.22417.

42. Bagni, C.; Zukin, R.S. A Synaptic Perspective of Fragile X Syndrome and Autism Spectrum Disorders. *Neuron* **2019**, *101*, 1070–1088, doi:10.1016/j.neuron.2019.02.041.

43. Kasai, H.; Ziv, N.E.; Okazaki, H.; Yagishita, S.; Toyoizumi, T. Spine Dynamics in the Brain, Mental Disorders and Artificial Neural Networks. *Nat Rev Neurosci* **2021**, *22*, 407–422, doi:10.1038/s41583-021-00467-3.

44. Irwin, S.A. Dendritic Spine Structural Anomalies in Fragile-X Mental Retardation Syndrome. *Cerebral Cortex* **2000**, *10*, 1038–1044, doi:10.1093/cercor/10.10.1038.

45. He, C.X.; Portera-Cailliau, C. The Trouble with Spines in Fragile X Syndrome: Density, Maturity and Plasticity. *Neuroscience* **2013**, *251*, 120–128, doi:10.1016/j.neuroscience.2012.03.049.

46. Jawaid, S.; Kidd, G.J.; Wang, J.; Swetlik, C.; Dutta, R.; Trapp, B.D. Alterations in CA1 Hippocampal Synapses in a Mouse Model of Fragile X Syndrome. *Glia* **2018**, *66*, 789–800, doi:10.1002/glia.23284.

47. Grossman, A.W.; Elisseou, N.M.; McKinney, B.C.; Greenough, W.T. Hippocampal Pyramidal Cells in Adult Fmr1 Knockout Mice Exhibit an Immature-Appearing Profile of Dendritic Spines. *Brain Research* **2006**, *1084*, 158–164, doi:10.1016/j.brainres.2006.02.044.

48. Levenga, J.; de Vrij, F.M.S.; Buijsen, R.A.M.; Li, T.; Nieuwenhuizen, I.M.; Pop, A.; Oostra, B.A.; Willemsen, R. Subregion-Specific Dendritic Spine Abnormalities in the Hippocampus of Fmr1 KO Mice. *Neurobiology of Learning and Memory* **2011**, *95*, 467–472, doi:10.1016/j.nlm.2011.02.009.

49. Zeiss, C.J. Comparative Milestones in Rodent and Human Postnatal Central Nervous System Development. *Toxicol Pathol* **2021**, *49*, 1368–1373, doi:10.1177/01926233211046933.

50. Comery, T.A.; Harris, J.B.; Willems, P.J.; Oostra, B.A.; Irwin, S.A.; Weiler, I.J.; Greenough, W.T. Abnormal Dendritic Spines in Fragile X Knockout Mice: Maturation and Pruning Deficits. *Proc. Natl. Acad. Sci. U.S.A.* **1997**, *94*, 5401–5404, doi:10.1073/pnas.94.10.5401.

51. Hering, H.; Sheng, M. Dentritic Spines : Structure, Dynamics and Regulation. *Nat Rev Neurosci* **2001**, *2*, 880–888, doi:10.1038/35104061.

52. Mundel, P.; Heid, H.W.; Mundel, T.M.; Krüger, M.; Reiser, J.; Kriz, W. Synaptopodin: An Actin-Associated Protein in Telencephalic Dendrites and Renal Podocytes. *Journal of Cell Biology* **1997**, *139*, 193–204, doi:10.1083/jcb.139.1.193.

53. Czarnecki, K.; Haas, C.A.; Bas Orth, C.; Deller, T.; Frotscher, M. Postnatal Development of Synaptopodin Expression in the Rodent Hippocampus. *J. Comp. Neurol.* **2005**, *490*, 133–144, doi:10.1002/cne.20651.

54. Holbro, N.; Grunditz, Å.; Oertner, T.G. Differential Distribution of Endoplasmic Reticulum Controls Metabotropic Signaling and Plasticity at Hippocampal Synapses. *Proc. Natl. Acad. Sci. U.S.A.* **2009**, *106*, 15055–15060, doi:10.1073/pnas.0905110106.

55. Basnayake, K.; Mazaud, D.; Kushnireva, L.; Bemelmans, A.; Rouach, N.; Korkotian, E.; Holcman, D. Nanoscale Molecular Architecture Controls Calcium Diffusion and ER Replenishment in Dendritic Spines. *Sci. Adv.* **2021**, *7*, eabh1376, doi:10.1126/sciadv.abh1376.

56. Huber, K.M.; Gallagher, S.M.; Warren, S.T.; Bear, M.F. Altered Synaptic Plasticity in a Mouse Model of Fragile X Mental Retardation. *Proc. Natl. Acad. Sci. U.S.A.* **2002**, *99*, 7746–7750, doi:10.1073/pnas.122205699.

57. Catania, M.V.; D'Antoni, S.; Bonaccorso, C.M.; Aronica, E.; Bear, M.F.; Nicoletti, F. Group I Metabotropic Glutamate Receptors: A Role in Neurodevelopmental Disorders? *Mol Neurobiol* **2007**, *35*, 298–307, doi:10.1007/s12035-007-0022-1.

58. Fmr1 Knockout Mice: A Model to Study Fragile X Mental Retardation. The Dutch-Belgian Fragile X Consortium. *Cell* **1994**, *78*, 23–33.

59. Bagni, C.; Tassone, F.; Neri, G.; Hagerman, R. Fragile X Syndrome: Causes, Diagnosis, Mechanisms, and Therapeutics. *J. Clin. Invest.* **2012**, *122*, 4314–4322, doi:10.1172/JCI63141.

60. Grant, S.G. Synaptopathies: Diseases of the Synaptome. *Current Opinion in Neurobiology* **2012**, *22*, 522–529, doi:10.1016/j.conb.2012.02.002.

61. Imbriani, P.; Schirinzi, T.; Meringolo, M.; Mercuri, N.B.; Pisani, A. Centrality of Early Synaptopathy in Parkinson's Disease. *Front. Neurol.* **2018**, *9*, 103, doi:10.3389/fneur.2018.00103.

62. Shentu, Y.-P.; Huo, Y.; Feng, X.-L.; Gilbert, J.; Zhang, Q.; Liuyang, Z.-Y.; Wang, X.-L.; Wang, G.; Zhou, H.; Wang, X.-C.; et al. CIP2A Causes Tau/APP Phosphorylation, Synaptopathy, and Memory Deficits in Alzheimer's Disease. *Cell Reports* **2018**, *24*, 713–723, doi:10.1016/j.celrep.2018.06.009.

63. Iannuzzi, F.; Frisardi, V.; Annunziato, L.; Matrone, C. Might Fibroblasts from Patients with Alzheimer's Disease Reflect the Brain Pathology? A Focus on the Increased Phosphorylation of Amyloid Precursor Protein Tyr682 Residue. *Brain Sciences* **2021**, *11*, 103, doi:10.3390/brainsci11010103.

64. Bear, M.F.; Dölen, G.; Osterweil, E.; Nagarajan, N. Fragile X: Translation in Action. *Neuropsychopharmacol* **2008**, *33*, 84–87, doi:10.1038/sj.npp.1301610.

65. Bagni, C.; Greenough, W.T. From MRNP Trafficking to Spine Dysmorphogenesis: The Roots of Fragile X Syndrome. *Nat Rev Neurosci* **2005**, *6*, 376–387, doi:10.1038/nrn1667.

66. Thomazeau, A.; Bosch, M.; Essayan-Perez, S.; Barnes, S.A.; De Jesus-Cortes, H.; Bear, M.F. Dissociation of Functional and Structural Plasticity of Dendritic Spines during NMDAR and MGluR-Dependent Long-Term Synaptic Depression in Wild-Type and Fragile X Model Mice. *Mol Psychiatry* **2021**, *26*, 4652–4669, doi:10.1038/s41380-020-0821-6.

67. Alberini, C.M.; Travaglia, A. Infantile Amnesia: A Critical Period of Learning to Learn and Remember. *J Neurosci* **2017**, *37*, 5783–5795, doi:10.1523/JNEUROSCI.0324-17.2017.

68. Harris, K.M.; Jensen, F.E.; Tsao, B. Three-Dimensional Structure of Dendritic Spines and Synapses in Rat Hippocampus (CA1) at Postnatal Day 15 and Adult Ages: Implications for the Maturation of Synaptic Physiology and Long-Term Potentiation. *J Neurosci* **1992**, *12*, 2685–2705.

69. Sorra, K.E.; Fiala, J.C.; Harris, K.M. Critical Assessment of the Involvement of Perforations, Spinules, and Spine Branching in Hippocampal Synapse Formation. *J Comp Neurol* **1998**, *398*, 225–240.

70. Sorra, K.E.; Harris, K.M. Overview on the Structure, Composition, Function, Development, and Plasticity of Hippocampal Dendritic Spines. *Hippocampus* **2000**, *10*, 501–511, doi:10.1002/1098-1063(2000)10:5<501::AID-HIPO1>3.0.CO;2-T.

71. von Bohlen Und Halbach, O. Structure and Function of Dendritic Spines within the Hippocampus. *Ann Anat* **2009**, *191*, 518–531, doi:10.1016/j.aanat.2009.08.006.

72. Berning, S.; Willig, K.I.; Steffens, H.; Dibaj, P.; Hell, S.W. Nanoscopy in a Living Mouse Brain. *Science* **2012**, *335*, 551, doi:10.1126/science.1215369.

73. Chazeau, A.; Mehidi, A.; Nair, D.; Gautier, J.J.; Leduc, C.; Chamma, I.; Kage, F.; Kechkar, A.; Thoumine, O.; Rottner, K.; et al. Nanoscale Segregation of Actin Nucleation and Elongation Factors Determines Dendritic Spine Protrusion. *EMBO J* **2014**, *33*, 2745–2764, doi:10.15252/embj.201488837.

74. Maiti, P.; Manna, J.; Ilavazhagan, G.; Rossignol, J.; Dunbar, G.L. Molecular Regulation of Dendritic Spine Dynamics and Their Potential Impact on Synaptic Plasticity and Neurological Diseases. *Neuroscience & Biobehavioral Reviews* **2015**, *59*, 208–237, doi:10.1016/j.neubiorev.2015.09.020.

75. Booker, S.A.; Domanski, A.P.F.; Dando, O.R.; Jackson, A.D.; Isaac, J.T.R.; Hardingham, G.E.; Wyllie, D.J.A.; Kind, P.C. Altered Dendritic Spine Function and Integration in a Mouse Model of Fragile X Syndrome. *Nat Commun* **2019**, *10*, 4813, doi:10.1038/s41467-019-11891-6.

76. Liu, X.; Kumar, V.; Tsai, N.-P.; Auerbach, B.D. Hyperexcitability and Homeostasis in Fragile X Syndrome. *Front Mol Neurosci* **2021**, *14*, 805929, doi:10.3389/fnmol.2021.805929.

77. Scharkowski, F.; Frotscher, M.; Lutz, D.; Korte, M.; Michaelsen-Preusse, K. Altered Connectivity and Synapse Maturation of the Hippocampal Mossy Fiber Pathway in a Mouse Model of the Fragile X Syndrome. *Cereb Cortex* **2018**, *28*, 852–867, doi:10.1093/cercor/bhw408.

78. Runge, K.; Cardoso, C.; de Chevigny, A. Dendritic Spine Plasticity: Function and Mechanisms. *Front Synaptic Neurosci* **2020**, *12*, 36, doi:10.3389/fnsyn.2020.00036.

79. Bear, M.F.; Huber, K.M.; Warren, S.T. The MGluR Theory of Fragile X Mental Retardation. *Trends in Neurosciences* **2004**, *27*, 370–377, doi:10.1016/j.tins.2004.04.009.

80. D'Antoni, S.; Spatuzza, M.; Bonaccorso, C.M.; Musumeci, S.A.; Ciranna, L.; Nicoletti, F.; Huber, K.M.; Catania, M.V. Dysregulation of Group-I Metabotropic Glutamate (MGlu) Receptor Mediated Signalling in Disorders Associated with Intellectual Disability and Autism. *Neurosci Biobehav Rev* **2014**, *46 Pt 2*, 228–241, doi:10.1016/j.neubiorev.2014.02.003.